APPENDIX

Analytical methods

Whole-rock geochemical analyses. Samples were sawn from the altered and weathered rims, and then crushed to small blocks. Fresh blocks were picked and powdered to 200 meshes in an agate mill. Whole-rock major-element compositions were determined by the X-ray fluorescence (XRF) at the Analytical Laboratory, Beijing Research Institute of Uranium Geology, China. About 0.5 g of sample powders were mixed with 5 g $Li_2B_4O_7$ to make glass beads, which were analyzed on an Axios^{max} Mineral Spectrometer. The analytical uncertainties for major elements are generally within 1-5%. Ferrous iron was determined by the wet chemical titration method.

Whole-rock trace elements (including REE) were determined by an Element XR inductively coupled plasma-mass spectrometry (ICP-MS) at the Analytical Laboratory, Beijing Research Institute of Uranium Geology, China. About 50 mg powders were digested by a mixed acid of HNO_3 and HF in a Teflon vessel, which were heated within an oven at a temperature higher than 150 °C for at least 5 days. After driving the rest acid out of the vessels, the residues were changed to solutions, into which rhodium (Rh) was added as an internal standard. Internal standards (BCR-1, BHVO-1, AGV-2 and JB-1) were used for monitoring drift in mass response during mass spectrometric measurements. The precision was generally better than 10 % for most trace elements according to duplicate analyses on these standards.

Whole-rock Sr-Nd isotope analyses. Samples for Nd–Sr isotopic analysis were dissolved in Teflon bombs by $HF+HNO_3+HClO_4$ dissolution. Sr and Nd were separated using conventional ion exchange procedures as described by Wu et al. (2005). The Sr-Nd isotopic compositions were measured by thermal ionization mass spectrometry (TIMS) using an IsoProbe-T mass spectrometer at the Analytical Laboratory, Beijing Research Institute of Uranium Geology,

China. The $^{87}Sr/^{86}Sr$ ratios were normalized to $^{86}Sr/^{88}Sr = 0.1194$, and $^{143}Nd/^{144}Nd$ ratios to $^{146}Nd/^{144}Nd = 0.7219$. Total procedural blanks were <200 pg for Sr and <50 pg for Nd, and the estimated analytical uncertainties of the $^{147}Sm/^{144}Nd$ and $^{87}Rb/^{86}Sr$ ratios are <0.5%. The Sr standard solution (NBS 987) was analyzed and yielded an $^{87}Sr/^{86}Sr$ ratio of 0.710250 ± 14 (2σ), whereas the Nd standard solution (JMC) yielded a ratio of 0.512109 ± 6 (2σ) during data acquisition.

Zircon U-Pb dating and O isotope analyses by Secondary Ion Mass Spectrometer (SIMS). Zircons were separated from the crushed samples using standard density and magnetic separation techniques. They were handpicked carefully under a binocular microscope and mounted in epoxy resin, which were then polished until the grain centers were exposed. A zircon standard 91500, together with an in-house standard Qinghu, was mounted with zircon separates. Zircons were documented with transmitted and reflected light micrographs as well as cathodoluminescence (CL) images to reveal their internal structures, and the mount was vacuum-coated with high-purity gold prior to secondary ion mass spectrometry (SIMS) analysis at the Institute of Geology and Geophysics, Chinese Academy of Sciences (IGGCAS). Measurements of U, Th and Pb in zircons were conducted using the CAMECA ims-1280 ion microprobe at the IGGCAS. Uranium–Th–Pb isotopic ratios and absolute abundances were determined relative to the standard zircons 91500, analyses of which were interspersed with those of the unknown grains; operating and data processing procedures were similar to those described by Li et al. (2009). Zircon oxygen isotopes were measured using CAMECA ims-1280 SIMS, with an analytical procedure given by Li et al. (2010). Oxygen isotopes were obtained on the same spots of zircon grains that were previously analyzed for U-Pb age determinations. The Cs+ primary ion beam was accelerated at 10 kV, with an intensity of *ca* 2 nA. The spot size was about 20 μm in

diameter. The normal incidence electron flood gun was used to compensate for sample charging. Negative secondary ions were extracted with a -10 kV potential. Oxygen isotopes were measured using a multi-collection mode and the mass resolution used to measure oxygen isotopes was *ca* 2500. Measured $^{18}O/^{16}O$ ratios were normalized to Vienna Standard Mean Ocean Water compositions (VSMOW; $^{18}O/^{16}O$=0.0020052), and then corrected for instrumental mass fractionation (IMF) using the Penglai zircon standard. Measurement of the in-house standard Qinghu during the session yielded a value of 5.44 ‰ ± 0.06 ‰ (2SD, n=49), which is identical to the recommended value of 5.4 ‰ ± 0.2 ‰ (2SD; Li et al., 2013).

Whole-rock Li isotope analyses. Separation of Li for isotopic composition analysis was achieved by an organic solvent free two-step liquid chromatography procedure in a clean lab at the University of Science and Technology of China (USTC) following the procedure described by Gao and Casey (2012). All separations were monitored with ICP-MS analysis to guarantee both high Li yield (>99.8% recovery) and low Na/Li ratio (<0.5). The final concentration of Li in the solutions utilized for MC-ICPMS analyses was targeted to be about 50–100 ppb to ensure the best precision and accuracy. The total procedural blank determined for both the column procedure alone and the combined sample digestion and column procedure were less than ~0.03 ng of Li. Compared with the ~200–5000 ng Li used for our analysis, the blank correction is not significant at the uncertainty levels achieved. We report results as $\delta^7Li = ((^7Li/^6Li)_{sample} / (^7Li/^6Li)_{standard} - 1)) \times 1000$ relative to the L-SVEC Li-isotope standard (Flesch et al., 1973).

The lithium isotopic compositions were analysed at USTC. The lithium isotopic compositions were analysed on a *Neptune Plus* MC-ICP-MS on wet plasma mode using X skimmer cone and Jet sample cone. Samples were introduced through a low-flow PFA nebulizer (~50 μL/min) coupled with a quartz spray chamber. The two Li isotopes (^7Li and ^6Li) were

measured simultaneously in two opposing Faraday cups. Each sample analysis was bracketed before and after by 100 ppb L-SVEC standard. For a solution with 100 ppb Li and solution uptake rate of 50 μL/min, the typical intensity of ^{7}Li is about 8 V. The in-run precision on $^{7}Li/^{6}Li$ measurements is ≤0.2‰ for one block of 60 ratios. The external precision, based on long-term analysis of in-house standards (Li-QCUSTC = +8.8 ± 0.2‰ (2SD, n = 161)) is ≤0.5‰. For international rock standards, repeat analysis at USTC yielded +4.4 ± 0.3‰ (2SD, n = 8) for BHVO-2, −0.8 ± 0.3‰ (2SD, n = 29) for GSP-2, and +5.9 ± 0.5‰ (2SD, n = 9) for AGV-1, which are within uncertainty of previously published results (e.g., Rudnick et al., 2004; Gao and Casey, 2012; Lin et al., 2016).

Whole-rock B isotope analyses. Before powdered whole-rock samples were used to determine the B contents and isotopic compositions, a 2M HCl leaching for 5 h was performed to exclude contamination of posteruption alteration following the procedure of Tanaka and Nakamura (2005). The B concentration of these samples was measured by ICP-atomic emission spectrometry at the Guangzhou Institute of Geochemistry, Chinese Academy of Sciences (GIGCAS), following the methods of Wei et al. (2013). Boron concentration data have uncertainties of ~±10% (1σ). Boron isotopes were determined with splits of the same samples used for B concentration measurements following the procedure of Wei et al. (2013), by digestion of powdered whole-rock samples in HF, purification by ion exchange, and analysis by MC-ICP-MS at GIGCAS. Boron isotopic compositions are reported as $\delta^{11}B$, the per mil deviation of $^{11}B/^{10}B$ from that of SRM 951 boric acid. Precision and accuracy are estimated conservatively as ± 0.64‰, based on the replicate measurements of reference material JB-3 ($\delta^{11}B$ = +6.03 ± 0.41‰ (2σ), n = 15 analyses with independent chemistry).

Whole-rock Mg isotope analyses. Magnesium isotopes were measured using a Thermo Scientific *Neptune Plus* MC-ICPMS following similar methods of An et al. (2014) at USTC and of Ke et al. (2016) at the Isotope Geochemistry Laboratory, China University of Geosciences, Beijing, respectively. Whole-rock powders were fully digested to obtain ~10 μg Mg for chemical purification. A mixture of concentrated HF-HNO_3-HCL was used for digestion. Mg purification was performed in Savillex microcolumns loaded with 2 ml of Bio-Rad AG50W-X8 resin. The purified solutions were first analyzed for Mg concentration using MC-ICP-MS by comparing ^{24}Mg signals with those of standards with known concentrations. Total procedure blank was <10 ng for Mg, which accounts for negligible portions of the collected Mg (<0.001%). Mg isotope measurements were carried out in low resolution modes under wet plasma conditions. About 7 V signal of ^{24}Mg can be yielded for solutions containing ~400 ng/g Mg. Instrumental mass fractionation was corrected by using sample-standard bracketing (SSB) method for Mg isotopes.

The Mg isotope results are reported using the standard δ notation relative to DSM-3. Uncertainties for $\delta^{25}Mg$ and $\delta^{26}Mg$ of standards and samples are given as two standard deviations (2sd) based on repeated measurements. The long term external precision is better than ± 0.06 ‰ for $\delta^{26}Mg$ values (Ke et al., 2016). During the analytical session, the $\delta^{26}Mg$ results of AGV-2 (-0.23 ± 0.06‰), BHVO-2 (-0.23 ± 0.02 ‰), GSP-2 (0.03 ± 0.03‰) and G-2 (-0.165 ± 0.03 ‰) are all identical within error with the established values (An et al., 2014; Teng, 2017).

References

An, Y., Wu, F., Xiang, Y., Nan, X., Yu, X., Yang, J., Yu, H., Xie, L., and Huang, F., 2014, High-precision Mg isotope analyses of low-Mg rocks by MC-ICP-MS: Chemical Geology, v. 390, p. 9-21.

Flesch, G. D., Anderson, A. R., and Svec, H. J., 1973, A secondary isotopic standard for $^{6}Li/^{7}Li$ determinations: International Journal of Mass Spectrometry and Ion Physics, v. 12, no. 3, p. 265-272.

Gao, Y., and Casey, J. F., 2012, Lithium Isotope Composition of Ultramafic Geological Reference Materials JP-1 and DTS-2: Geostandards and Geoanalytical Research, v. 36, no. 1, p. 75-81.

Ke, S., Teng, F.-Z., Li, S.-G., Gao, T., Liu, S.-A., He, Y., and Mo, X., 2016, Mg, Sr, and O isotope geochemistry of syenites from northwest Xinjiang, China: Tracing carbonate recycling during Tethyan oceanic subduction: Chemical Geology, v. 437, p. 109-119.

Laurent, O., Martin, H., Moyen, J. F., and Doucelance, R., 2014, The diversity and evolution of late-Archean granitoids: Evidence for the onset of "modern-style" plate tectonics between 3.0 and 2.5Ga: Lithos, v. 205, p. 208-235, https://doi.org/10.1016/j.lithos.2014.06.012.

Li, X., Tang, G., Gong, B., Yang, Y., Hou, K., Hu, Z., Li, Q., Liu, Y., and Li, W., 2013, Qinghu zircon: A working reference for microbeam analysis of U-Pb age and Hf and O isotopes: Chinese Science Bulletin, v. 58, no. 36, p. 4647-4654.

Li, X.-H., Liu, Y., Li, Q.-L., Guo, C.-H., and Chamberlain, K. R., 2009, Precise determination of Phanerozoic zircon Pb/Pb age by multicollector SIMS without external standardization: Geochemistry, Geophysics, Geosystems, v. 10, no. 4. https://doi.org/10.1029/2009GC002400.

Li, X.-H., Long, W.-G., Li, Q.-L., Liu, Y., Zheng, Y.-F., Yang, Y.-H., Chamberlain, K. R., Wan, D.-F., Guo, C.-H., Wang, X.-C., and Tao, H., 2010, Penglai Zircon Megacrysts: A Potential New Working Reference Material for Microbeam Determination of Hf–O Isotopes and U–Pb Age: Geostandards and Geoanalytical Research, v. 34, no. 2, p. 117-134.

Lin, J., Liu, Y., Hu, Z., Yang, L., Chen, K., Chen, H., Zong, K., and Gao, S., 2016, Accurate determination of lithium isotope ratios by MC-ICP-MS without strict matrix-matching by using a novel washing method: Journal of Analytical Atomic Spectrometry, v. 31, no. 2, p. 390-397.

Maniar, P. D., and Piccoli, P. M., 1989, Tectonic discrimination of granitoids: Geological Society of America Bulletin, v. 101, no. 5, p. 635-643.

Rudnick, R. L., Tomascak, P. B., Njo, H. B., and Gardner, L. R., 2004, Extreme lithium isotopic fractionation during continental weathering revealed in saprolites from South Carolina: Chemical Geology, v. 212, no. 1, p. 45-57.

Tanaka, R., and Nakamura, E., 2005, Boron isotopic constraints on the source of Hawaiian shield lavas: Geochimica et Cosmochimica Acta, v. 69, no. 13, p. 3385-3399.

Teng, F.-Z., 2017, Magnesium Isotope Geochemistry: Reviews in Mineralogy and Geochemistry, v. 82, no. 1, p. 219-287.

Wei, G., Wei, J., Liu, Y., Ke, T., Ren, Z., Ma, J., and Xu, Y., 2013, Measurement on high-precision boron isotope of silicate materials by a single column purification method and MC-ICP-MS: Journal of Analytical Atomic Spectrometry, v. 28, no. 4, p. 606-612.

Wu, F. Y., Yang, J. H., Wilde, S. A., and Zhang, X. O., 2005, Geochronology, petrogenesis and tectonic implications of Jurassic granites in the Liaodong Peninsula, NE China: Chemical Geology, v. 221, no. 1-2, p. 127-156.

Supplementary figure caption

Figure S1. Simplified granitoid map showing the distribution of proposed S-type, I-type (with or without an adakite affinity), A-type and sanukitoid-like high Ba-Sr granitoids in the

Songpan-Ganzi terrane, eastern Tibetan Plateau. Abbreviations as follows: KQQ, Kunlun‐Qaidam‐Qilian terrane; HX, Hoh‐Xil terrane; SG, Songpan‐Ganzi terrane; GI, Greater India; WKT, West Kunlun thrust belt; NQLT, North Qilian Shan thrust belt; MFT, Main Frontal thrust belt; LMST, Longmeng Shan thrust belt.

Figure S2. A: Na_2O (wt. %) *vs* K_2O (wt. %). B: The 2 A/CNK (molar $Al_2O_3/[CaO+Na_2O+K_2O]$ ratio) vs. Na_2O/K_2O ratio vs. 2 FMSB $(FeOt+MgO)_{wt.\%} * (Sr+Ba)_{wt.\%}$ diagram (Laurent et al., 2014). C: SiO_2 (wt. %) *vs* zircon $\delta^{18}O$ values (‰). D: SiO_2 (wt. %) *vs* whole-rock $\delta^{7}Li$ (‰). E: SiO_2 (wt. %) *vs* whole-rock $\delta^{11}B$ (‰). F: SiO_2 (wt. %) *vs* whole-rock $\delta^{26}Mg$ values (‰).

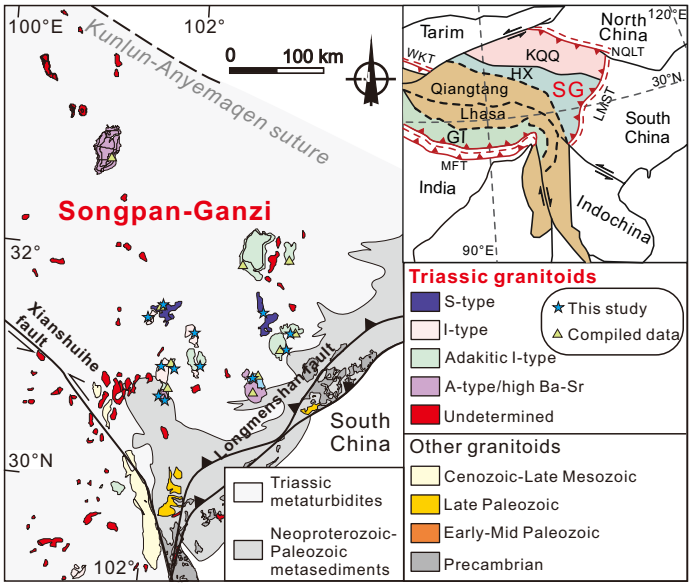
100°E
102°
0
100 km
Kunlun-Anyemaqen suture
Songpan-Ganzi
32°
Xianshuihe fault
Longmenshan fault
South China
30°N
102°
Triassic metaturbidites
Neoproterozoic-Paleozoic metasedimentes
Tarim
North China
120°E
WKT
KQQ
NQLT
HX
SG
30°N
Qiangtang
Lhasa
GT
LMST
South China
MFT
India
Indochina
90°E
Triassic granitoids
S-type
I-type
Adakitic I-type
A-type/high Ba-Sr
Undetermined
This study
Compiled data
Other granitoids
Cenozoic-Late Mesozoic
Late Paleozoic
Early-Mid Paleozoic
Precambrian

Figure S1

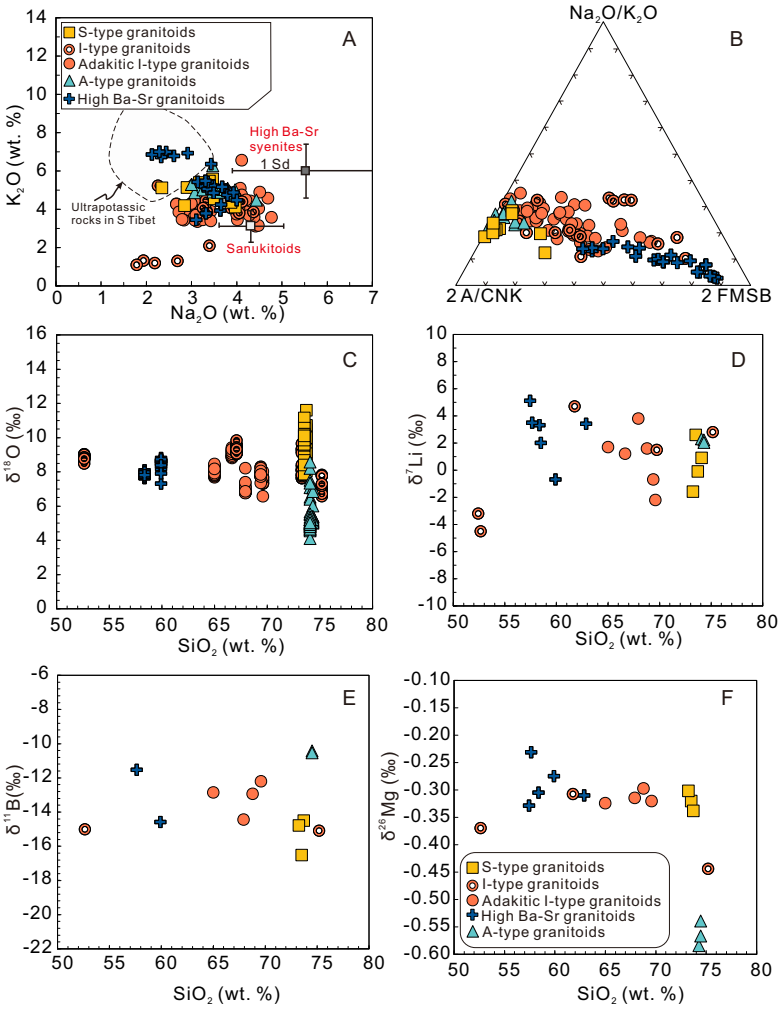
A
S-type granitoids
I-type granitoids
Adakitic I-type granitoids
A-type granitoids
High Ba-Sr granitoids
High Ba-Sr syenites
1 Sd
Ultrapotassic rocks in S Tibet
Sanukitoids
K2O (wt. %)
Na2O (wt. %)
B
Na2O/K2O
2 A/CNK
2 FMSB
C
δ18O (‰)
SiO2 (wt. %)
D
δ7Li (‰)
SiO2 (wt. %)
E
δ11B(‰)
SiO2 (wt. %)
F
δ26Mg (‰)
SiO2 (wt. %)
S-type granitoids
I-type granitoids
Adakitic I-type granitoids
High Ba-Sr granitoids
A-type granitoids

Figure S2